

INTERMITTENT PROCESS ANALYSIS WITH SCATTERING MOMENTS

BY JOAN BRUNA, STÉPHANE MALLAT¹,
EMMANUEL BACRY AND JEAN-FRANÇOIS MUZY

*New York University, École Normale Supérieure, CNRS, Ecole
Polytechnique, and CNRS, Ecole Polytechnique and CNRS, Université de
Corse*

Scattering moments provide nonparametric models of random processes with stationary increments. They are expected values of random variables computed with a nonexpansive operator, obtained by iteratively applying wavelet transforms and modulus nonlinearities, which preserves the variance. First- and second-order scattering moments are shown to characterize intermittency and self-similarity properties of multiscale processes. Scattering moments of Poisson processes, fractional Brownian motions, Lévy processes and multifractal random walks are shown to have characteristic decay. The Generalized Method of Simulated Moments is applied to scattering moments to estimate data generating models. Numerical applications are shown on financial time-series and on energy dissipation of turbulent flows.

1. Introduction. Defining nonparametric models of non-Gaussian stationary processes remains a core issue of probability and statistics. Computing polynomial moments is a tempting strategy which suffers from the large variance of high order moment estimators. Image and audio textures are examples of complex processes with stationary increments, which can be discriminated from a single realization by the human brain. Yet, the amount of samples is often not sufficient to reliably estimate polynomial moments of degree more than 2. These non-Gaussian processes often have a long range dependency, and some form of intermittency generated by randomly distributed bursts of transient structures at multiple scales. Intermittency

Received November 2013; revised May 2014.

¹Supported by the ANR 10-BLAN-0126 and ERC InvariantClass 320959 grants.

AMS 2000 subject classifications. 62M10, 62M15, 62M40.

Key words and phrases. Multifractal, intermittency, wavelet analysis, spectral analysis, Generalized method of moments.

<p>This is an electronic reprint of the original article published by the Institute of Mathematical Statistics in <i>The Annals of Statistics</i>, 2015, Vol. 43, No. 1, 323–351. This reprint differs from the original in pagination and typographic detail.</p>
--

is an ill-defined mathematical notion, which is used in physics to describe those irregular bursts of large amplitude variations, appearing, for example, in turbulent flows [39]. Multiscale intermittency appears in other domains such as network traffics, financial time series, geophysical and medical data.

Intermittency is created by heavy tail processes, such as Lévy processes. It produces large if not infinite polynomial moments of degree larger than two, and empirical estimations of second-order moments have a large variance. These statistical instabilities can be reduced by calculating expected values of nonexpansive operators in mean-square norm, which reduce the variance of empirical estimation. Scattering moments are computed with such a nonexpansive operator. They are calculated by iteratively applying wavelet transforms and modulus nonlinearities [25]. This paper shows that they characterize self-similarity and intermittency properties of processes with stationary increments. These properties are studied by computing the scattering moments of Poisson processes, fractional Brownian motions, Lévy processes and multifractal cascades, which all have very different behavior. Scattering moments provide nonparametric descriptors, revealing nontrivial statistical properties of time series. The generalized method of simulated moments [16, 28] applied to scattering moments gives a parameter estimator for data generating models, and a goodness of fit under the appropriate statistical setting. Besides parameter estimation, a key challenge is to validate data generating models from small datasets.

Section 2 reviews the scaling properties of wavelet polynomial moments for fractal and multifractal processes. Scattering moments are defined and related to multi-scale intermittency properties. Poisson processes illustrate these first results. Section 3 proves that self-similar processes with stationary increments have normalized scattering moments which are stationary across scales. Gaussian processes are discriminated from non-Gaussian processes using second-order scattering moments. Results on fractional Brownian motion and stable Lévy processes illustrate the multi-scale intermittency properties of these moments. Section 4 extends these results to self-similar multifractal cascades [5, 26, 27].

Section 5 applies scattering moments to estimate model parameters. It introduces a scattering moment estimator whose variance is bounded. Parameters of data generating models are estimated from scattering moments with the generalized method of simulated moments [16, 28]. Scattering moments of financial time-series and turbulence energy dissipation are computed from numerical data. Models based on fractional Brownian, Lévy stable and multifractal cascade processes are evaluated with a J-test. Computations can be reproduced with a software available at www.di.ens.fr/data/software/scatnet.

Notation. We denote $\{X(t)\}_t \stackrel{d}{=} \{Y(t)\}_t$ the equality of all finite-dimensional distributions. The dyadic scaling of $X(t)$ is written $L_j X(t) =$

$X(2^{-j}t)$. If $X(t)$ is stationary then $\mathbf{E}(X(t))$ does not depend on t and is written $\mathbf{E}(X)$, and $\sigma^2(X) = \mathbf{E}(|X|^2) - \mathbf{E}(X)^2$. We denote $B(j) \simeq F(j), j \rightarrow \infty$ (resp., $j \rightarrow -\infty$) if there exists $C_1, C_2 > 0$ and $J \in \mathbb{Z}$ such that $C_1 \leq \frac{B(j)}{F(j)} \leq C_2$ for all $j > J$ (resp., for all $j < J$).

2. Scattering transform of intermittent processes.

2.1. Polynomial wavelet moments. Polynomial moments of wavelet coefficients reveal important multiscaling properties of fractals and multi-fractals [1, 3, 7, 17–19, 30, 32, 36, 37]. We consider real valued random processes $X(t)$ having stationary increments $X(t) - X(t - \tau)$ for any $\tau \in \mathbb{R}$. A wavelet $\psi(t)$ is a function of zero average $\int \psi(t) dt = 0$ with $|\psi(t)| = O((1 + |t|^2)^{-1})$. The wavelet transform of $X(t)$ at a scale 2^j is defined for all $t \in \mathbb{R}$ by

$$(1) \quad X \star \psi_j(t) = \int X(u) \psi_j(t - u) du,$$

where $\forall j \in \mathbb{Z}, \psi_j(t) = 2^{-j} \psi(2^{-j}t)$ is a dilated version of ψ . A wavelet $\psi(t)$ is said to have q vanishing moments if $\int t^k \psi(t) dt = 0$ for $0 \leq k < q$. Since $\int \psi(t) dt = 0$, if X has stationary increments, then one can verify that $X \star \psi_j(t)$ is a stationary process [32]. The dyadic wavelet transform of $X(t)$ is

$$(2) \quad WX = \{X \star \psi_j\}_{j \in \mathbb{Z}}.$$

A wavelet ψ satisfies the Littlewood–Paley condition if its Fourier transform Ψ satisfies for all $\omega \neq 0$

$$(3) \quad \sum_{j=-\infty}^{\infty} |\Psi(2^j \omega)|^2 + \sum_{j=-\infty}^{\infty} |\Psi(-2^j \omega)|^2 = 2.$$

If $X(t)$ is a real valued stationary process with $\mathbf{E}(|X(t)|^2) < \infty$, then the wavelet transform energy equals the process variance $\sigma^2(X)$

$$(4) \quad \mathbf{E}(\|WX\|^2) = \sum_{j \in \mathbb{Z}} \mathbf{E}(|X \star \psi_j|^2) = \sigma^2(X).$$

This is proved by expressing $\mathbf{E}(|X \star \psi_j|^2)$ in terms of the power spectrum of X and inserting (3).

The decay of monomial wavelet moments across scales can be related to the distributions of pointwise Holder exponents [3, 19, 32, 36, 37]. Moments of degree q define a scaling exponent $\zeta(q)$ such that

$$\mathbf{E}(|X \star \psi_j(t)|^q) \simeq 2^{j\zeta(q)}.$$

Monofractals such as fractional Brownian motions have linear scaling exponents: $\zeta(q) = q\zeta(1)$. These Gaussian processes have realizations which are

uniformly regular. The curvature of $\zeta(q)$ is related to the presence of different pointwise Holder exponents, in each realization of X [7, 17, 18]. It has been interpreted as a measurement of intermittency [1]. Such properties cannot be obtained with Fourier moments, which depend upon the global Holder regularity of each realization, as opposed to pointwise Holder exponents. However, as q deviates from 1, estimations of moments become progressively more unstable which limits the application of this multifractal formalism to very large data sets.

2.2. Scattering moments. Scattering moments are expected values of a nonexpansive transformation of the process. They are computed with a cascade of wavelet transforms and modulus nonlinearities [25]. We review their elementary properties.

Let ψ be a \mathbf{C}^1 , complex wavelet, whose real and imaginary parts are orthogonal, and have the same $\mathbf{L}^2(\mathbb{R})$ norm. In this paper, we impose that ψ has a compact support normalized to $[-1/2, 1/2]$, which simplifies the proofs. However, most results remain valid without this compact support hypothesis. We consider wavelets ψ which are nearly analytic, in the sense that their Fourier transform $\Psi(\omega)$ is nearly zero for $\omega < 0$. The compact support hypothesis prevents it from being strictly zero. All numerical computations in the paper are performed with the compactly supported complex wavelets of Selesnick [34], whose real and imaginary parts have 4 vanishing moments and are nearly Hilbert transform pairs.

Let $X(t)$ be a real valued process with stationary increments having finite first-order moments: $\mathbf{E}(|X(t) - X(t - \tau)|) < \infty$ for all $\tau \in \mathbb{R}$. The wavelet transform $X \star \psi_{j_1}(t)$ is a complex stationary random process. First-order scattering moments are defined by

$$\forall j_1 \in \mathbb{Z}, \quad \overline{S}X(j_1) = \mathbf{E}(|X \star \psi_{j_1}|).$$

First-order scattering moments do not capture the time variability of wavelet coefficients $X \star \psi_{j_1}(t)$. This information is partly provided by second-order scattering moments computed from the wavelet transform of each $|X \star \psi_{j_1}(t)|$:

$$\forall (j_1, j_2) \in \mathbb{Z}^2, \quad \overline{S}X(j_1, j_2) = \mathbf{E}(|X \star \psi_{j_1}| \star \psi_{j_2}).$$

These moments measure the average multi-scale time variations of $|X \star \psi_{j_1}|$, with a second family of wavelets ψ_{j_2} . If $j_2 < j_1$ then $\overline{S}X(j_1, j_2)$ has a fast decay to zero as $j_1 - j_2$ increases. Its amplitudes depend on the wavelet properties as opposed to the properties of X . Indeed, if $|\psi|$ is \mathbf{C}^p and has p vanishing moments then $|X \star \psi_{j_1}|$ is typically almost everywhere \mathbf{C}^p so $\overline{S}X(j_1, j_2) = \mathbf{E}(|X \star \psi_{j_1}| \star \psi_{j_2}) = O(2^{p(j_2 - j_1)})$. We thus concentrate on scattering moments for $j_2 > j_1$.

The expected value of second-order moments averages the time variability of $\|X \star \psi_{j_1} \star \psi_{j_2}(t)\|$. This lost information can be recovered by calculating the wavelet transform of $\|X \star \psi_{j_1} \star \psi_{j_2}(t)\|$ for each (j_1, j_2) . Iterating this process computes scattering moments at any order $m \geq 1$:

$$(5) \quad \forall (j_1, \dots, j_m) \in \mathbb{Z}^m, \quad \overline{S}X(j_1, \dots, j_m) = \mathbf{E}(\|X \star \psi_{j_1} \star \dots \star \psi_{j_m}\|).$$

If $\mathbf{E}(|X(t) - X(t - \tau)|) < \infty$ for all $\tau \in \mathbb{R}$, then $\mathbf{E}(|X \star \psi_{j_1}|) < \infty$ and one can verify by induction on m that $\overline{S}X(j_1, \dots, j_m) < \infty$.

The vector of all scattering moments of X defines a nonparametric representation

$$\overline{S}X = \{\overline{S}X(j_1, \dots, j_m) : \forall (j_1, \dots, j_m) \in \mathbb{Z}^m, \forall m \in \mathbb{N}^*\}.$$

Its ℓ_2 norm is

$$(6) \quad \|\overline{S}X\|^2 = \sum_{m=1}^{\infty} \sum_{(j_1, \dots, j_m) \in \mathbb{Z}^m} |\overline{S}X(j_1, \dots, j_m)|^2.$$

Since the wavelet transform preserves the variance in (4) and the modulus operator obviously also preserves the variance, each wavelet transform and modulus iteration preserves the variance. If $\mathbf{E}(|X|^2) < \infty$ then by applying (4), we verify [25] by induction on l that scattering coefficients satisfy

$$\begin{aligned} & \sum_{m=1}^{l-1} \sum_{(j_1, \dots, j_m) \in \mathbb{Z}^m} |\overline{S}X(j_1, \dots, j_m)|^2 \\ &= \sigma^2(X) - \sum_{(j_1, \dots, j_l) \in \mathbb{Z}^l} \mathbf{E}(\|X \star \psi_{j_1} \star \dots \star \psi_{j_l}\|^2), \end{aligned}$$

with $\sigma^2(X) = \mathbf{E}(|X|^2) - |\mathbf{E}(X)|^2$. It results that $\|\overline{S}X\|^2 \leq \sigma^2(X)$. Numerical experiments indicate that for large classes of ergodic stationary processes, $\sum_{(j_1, \dots, j_l) \in \mathbb{Z}^l} \mathbf{E}(\|X \star \psi_{j_1} \star \dots \star \psi_{j_l}\|^2)$ converges to zero as 2^l increases. It then implies $\|\overline{S}X\|^2 = \sigma^2(X)$. Similarly to the Fourier power spectrum, the ℓ^2 norm of scattering moments is then equal to the variance. However, this remains a conjecture [25].

The scattering norm (6) can be approximated with a summation restricted to moments of order $m = 1, 2$, because higher order scattering moments usually have a much smaller energy [2, 9]. First- and second-order scattering moments applied to image and audio textures as well as intrapartum electrocardiograms for fetal monitoring provide state of the art classification errors [2, 9, 13, 35], but these results are strictly numerical. These algorithms are implemented with deep convolutional neural network structures [24]. In the following, we concentrate on the mathematical properties of first- and second-order scattering moments, which characterize self-similarity and intermittency properties.

2.3. *Normalized scattering and intermittency.* Scattering moments are normalized to increase their invariance properties. Invariance to multiplicative factors is obtained with

$$\tilde{S}X(j_1) = \frac{\overline{S}X(j_1)}{\overline{S}X(0)} = \frac{\mathbf{E}(|X \star \psi_{j_1}|)}{\mathbf{E}(|X \star \psi|)}.$$

Second-order scattering moments are normalized by their first-order moment:

$$\tilde{S}X(j_1, j_2) = \frac{\overline{S}X(j_1, j_2)}{\overline{S}X(j_1)} = \frac{\mathbf{E}(|X \star \psi_{j_1} \star \psi_{j_2}|)}{\mathbf{E}(|X \star \psi_{j_1}|)}.$$

This can be rewritten

$$\tilde{S}X(j_1, j_2) = \overline{S}\tilde{X}_{j_1}(j_2) = \mathbf{E}(|\tilde{X}_{j_1} \star \psi_{j_2}|) \quad \text{with } \tilde{X}_{j_1} = \frac{|X \star \psi_{j_1}|}{\mathbf{E}(|X \star \psi_{j_1}|)}.$$

If X has stationary increments then \tilde{X}_{j_1} is a normalized stationary process providing the occurrence of “burst” of activity at the scale 2^{j_1} . Normalized second-order moments $\tilde{S}X(j_1, j_2)$ thus measure the time variability of these burst of activity over time scales $2^{j_2} \geq 2^{j_1}$, which gives multi-scale measurements of intermittency.

Intermittency aims at capturing the geometric distribution of burst of high variability in each realization of X . It is not modified by the action of derivative operators, which are translation invariant. We verify that this invariance property holds for normalized second-order moments. Let d^α be a fractional derivative defined by the multiplication by $(i\omega)^\alpha$ in the Fourier domain. Since

$$d^\alpha X \star \psi_{j_1}(t) = 2^{-\alpha j_1} X \star \psi_{j_1}^\alpha(t),$$

where $\psi^\alpha = d^\alpha \psi$ and $\psi_{j_1}^\alpha(t) = 2^{-j_1} \psi^\alpha(2^{-j_1} t)$, it results that

$$(7) \quad \overline{S}d^\alpha X(j_1) = 2^{-\alpha j_1} \mathbf{E}(|X \star \psi_{j_1}^\alpha|)$$

and

$$(8) \quad \tilde{S}d^\alpha X(j_1, j_2) = \frac{\mathbf{E}(|X \star \psi_{j_1}^\alpha \star \psi_{j_2}|)}{\mathbf{E}(|X \star \psi_{j_1}^\alpha|)}.$$

If $X(t)$ has no oscillating singularity [21], then its wavelet coefficients calculated with ψ and ψ^α have the same asymptotic decay, so

$$(9) \quad \overline{S}d^\alpha X(j_1) \simeq 2^{-\alpha j_1} \overline{S}X(j_1) \quad \text{and} \quad \tilde{S}d^\alpha X(j_1, j_2) \simeq \tilde{S}X(j_1, j_2).$$

Modifications of regularity produced by derivative operators affect the decay of first-order scattering moments but not the decay of normalized second-order moments. Fractional Brownian motions illustrate these properties in Section 3.2.

Global intermittency parameters computed with wavelet moments can be related to normalized second-order scattering moments. If $\mathbf{E}(|X \star \psi_j|^q) \simeq 2^{j\zeta(q)}$ then intermittency is measured by the curvature of $\zeta(q)$. If one quantifies it by $\zeta(2) - 2\zeta(1)$, we verify from (4) that

$$2^{j(\zeta(2)-2\zeta(1))} \simeq \frac{\mathbf{E}(|X \star \psi_j|^2)}{\mathbf{E}(|X \star \psi_j|)^2} \geq 1 + \sum_{j_2=-\infty}^{+\infty} |\tilde{S}X(j, j_2)|^2.$$

It results that if $\sum_{j_2=-\infty}^{+\infty} \tilde{S}X(j, j_2)^2 \simeq 2^{j\beta}$ as $j \rightarrow -\infty$ with $\beta < 0$, then $\zeta(2) - 2\zeta(1) < 0$. However, these moments eliminate the dependency on the scale parameter 2^{j^2} , which provides a finer multi-scale characterization of the intermittency regularity. This dependency upon 2^{j^2} is studied in the next sections and is used for model selection in Section 5.

2.4. Scattering Poisson processes. The properties of scattering moments are illustrated over a Poisson process, which is a simple Lévy process with stationary increments. A homogeneous Poisson process $\{X(t), t \geq 0\}$ has increments $X(t + \Delta) - X(t)$ which count the number of occurrence of events in $]t, t + \Delta]$, and have a Poisson distribution of intensity λ . Figure 1(a)

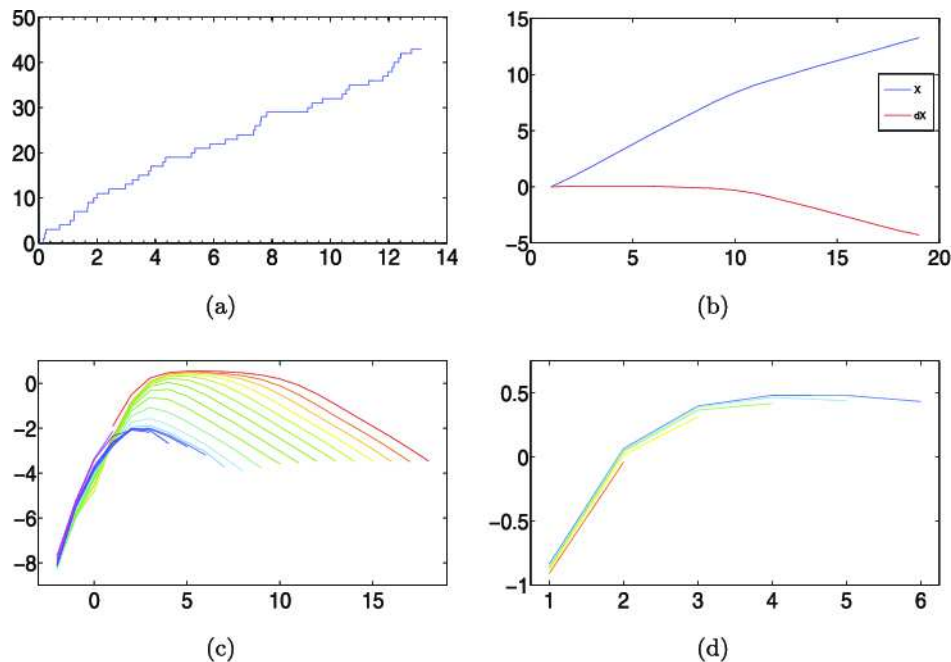


FIG. 1. (a) Realization of a Poisson process $X(t)$ of intensity $\lambda = 10^{-4}$. (b) $\log_2 \tilde{S}X(j)$ and $\log_2 \tilde{S}dX(j)$ as a function of j . (c) $\log_2 \tilde{S}X(j_1, j_2)$ as a function of $j_2 - j_1$ for several values of j_1 . (d) The same curves as in (c), but restricted to $j_2 < -\log_2(\lambda) - 1$.

shows an example. The following proposition gives the decay of first- and second-order scattering moments of Poisson processes.

THEOREM 2.1. *If X is a Poisson process of intensity λ and $\bar{\psi}(t) = \int_0^t \psi(u) du$ then for all $j_1 \leq j_2$*

$$(10) \quad \bar{S}X(j_1) = 2^{j_1} \lambda \|\bar{\psi}\|_1 (1 + O(2^{j_1} \lambda)),$$

$$(11) \quad \lim_{j_1 \rightarrow \infty} 2^{-j_1/2} \bar{S}X(j_1) = C \lambda^{1/2} > 0,$$

where C depends only upon the wavelet ψ , and

$$(12) \quad \tilde{S}X(j_1, j_2) = \frac{\|\bar{\psi}\|_1 \|\psi_{j_2-j_1}\|_1}{\|\bar{\psi}\|_1} (1 + O(\lambda 2^{j_1}) + O(\lambda 2^{j_2})),$$

$$(13) \quad \lim_{j_2 \rightarrow \infty} 2^{j_2/2} \tilde{S}X(j_1, j_2) = C' > 0.$$

The proof is in Appendix A in [10]. At scales $2^{j_1} \leq 2^{j_2} \ll \lambda^{-1}$, the Poisson process typically has 1 jump over the support of each wavelet, which implies (10). When $2^{j_1} \gg \lambda^{-1}$, Appendix A proves that $X \star \psi_{j_1}(t)$ converges to the wavelet transform of a Gaussian white noise of variance $\lambda 2^{j_1}$, which implies (11).

When $2^{j_2} \ll \lambda^{-1}$, (12) implies that

$$\lim_{j_1 \rightarrow -\infty} \tilde{S}X(j_1, j_2) = \|\psi\|_1 (1 + O(2^{j_2} \lambda)).$$

This convergence to a constant indicates a high degree of intermittency, because fine scale wavelets see individual Diracs occurring randomly. This property is observed in Figure 1(d), which gives $\log_2 \tilde{S}X(j_2 - j_1, j_2)$ as a function of $j_2 - j_1$. These curves overlap for different j_1 , and converge to $\|\psi\|_1$.

If $2^{j_2} \gg \lambda^{-1}$ then $\tilde{S}X(j_1, j_2) \simeq 2^{-j_2/2}$. This decay is characteristic of Gaussian stationary processes, which are uniformly regular, and thus have no intermittency. This is further studied in Section 3.2 for fractional Brownian motions. Figure 1(c) verifies that $\tilde{S}X(j_2 - j_1, j_2)$ decays with a slope of $-1/2$ as a function of $j_2 - j_1$.

When going from X to dX then the sum of jumps is replaced by a measure which is a sum of Diracs. We verify from Appendix A that $\bar{S}dX(j_1) \simeq 2^{-j_1} \bar{S}X(j_1)$. This reflects the change of regularity. Figure 1(b) shows that the difference between the slopes of $\log_2 \bar{S}X(j_1)$ and $\log_2 \bar{S}dX(j_1)$ is indeed equal to 1. For normalized second-order moments, $\tilde{S}dX(j_1, j_2)$ is nearly equal to $\tilde{S}X(j_1, j_2)$, as expected from (8).

3. Self-similar processes. Second-order scattering moments of self-similar processes are proved to be stationary across scales. Fractional Brownian motions and Lévy stable processes are studied in Sections 3.2 and 3.3.

3.1. *Scattering self-similarity.* Self-similar processes of Hurst exponent H are stochastic processes $X(t)$ which are invariant in distribution under a scaling of space or time:

$$(14) \quad \forall s > 0, \quad \{X(st)\}_t \stackrel{d}{=} \{s^H X(t)\}_t.$$

We consider self-similar processes having stationary increments. Fractional Brownian motions and α -stable Lévy processes are examples of Gaussian and non-Gaussian self-similar processes with stationary increments.

If X is self-similar, then applying (14) with a change of variable $u' = 2^{-j}u$ in (1) proves that

$$\forall j \in \mathbb{Z}, \quad \{X \star \psi_j(t)\}_t \stackrel{d}{=} 2^{jH} \{X \star \psi(2^{-j}t)\}_t.$$

The following proposition proves that normalized second-order scattering moments can be written as a univariate function.

PROPOSITION 3.1. *If X is a self-similar process with stationary increments then for all $j_1 \in \mathbb{Z}$*

$$(15) \quad \tilde{S}X(j_1) = 2^{j_1 H},$$

and for all $(j_1, j_2) \in \mathbb{Z}^2$

$$(16) \quad \tilde{S}X(j_1, j_2) = \bar{S}\tilde{X}(j_2 - j_1) \quad \text{with } \tilde{X}(t) = \frac{|X \star \psi(t)|}{\mathbf{E}(|X \star \psi|)}.$$

PROOF. We write $L_j x(t) = x(2^{-j}t)$. Since $\psi_{j_1} = 2^{-j_1} L_{j_1} \psi$, a change of variables yields $L_{j_1} |X \star \psi| = |L_{j_1} X \star \psi_{j_1}|$, and hence

$$(17) \quad |X \star \psi_{j_1}| = L_{j_1} |L_{-j_1} X \star \psi| \stackrel{d}{=} 2^{j_1 H} L_{j_1} |X \star \psi|.$$

If $Y(t)$ is stationary, then $\mathbf{E}(L_j Y(t)) = \mathbf{E}(Y(t))$, which proves (15).

By cascading (17), we get

$$(18) \quad \forall (j_1, j_2), \quad ||X \star \psi_{j_1}| \star \psi_{j_2}| \stackrel{d}{=} 2^{j_1 H} L_{j_1} ||X \star \psi| \star \psi_{j_2 - j_1}|,$$

so $\bar{S}X(j_1, j_2) = 2^{j_1 H} \mathbf{E}(|X \star \psi| \star \psi_{j_2 - j_1})$. Together with (15), it proves (16). \square

Property (16) proves that if X is self-similar then $\tilde{S}X(j_1, j_1 + l)$ is a function of l , which can be interpreted as a stationary property across scales.

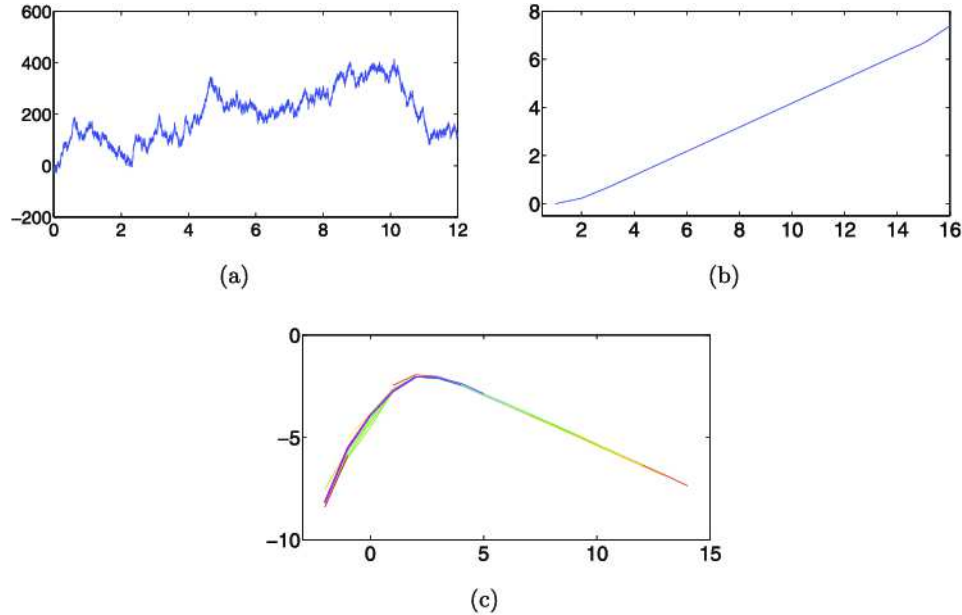


FIG. 2. (a) Realization of a Brownian motion $X(t)$. (b) $\log_2 \tilde{S}X(j_1)$ as a function of j_1 . (c) The curves $\log_2 \tilde{S}X(j_1, j_1 + l)$ as a function of l are identical for different j_1 .

This function of l is a scattering intermittency measure of the random process. A Brownian motion is a Gaussian self-similar process with a Hurst exponent $H = 1/2$. It results from (15) that $\log_2 \tilde{S}(j_1) = j_1/2$, which is illustrated by Figure 2(b). Figure 2(c) displays $\tilde{S}X(j_1, j_2)$ expressed as a function of $j_2 - j_1$, for different j_1 . The curves for different j_1 are equal, as proved by (15). When $j_2 - j_1 < 0$, $\tilde{S}X(j_1, j_2)$ increases with a slope which does not depend on X but on the number of vanishing moments and on the regularity of the wavelet ψ . For $j_2 - j_1 \geq 0$, the decay depends upon the property of X and satisfies $\tilde{S}X(j_1, j_2) \simeq 2^{-(j_2 - j_1)/2}$. The next section proves this result in the more general context of fractional Brownian motions, and shows that it reflects the fact that a Brownian motion is a Gaussian process.

3.2. Fractional Brownian motions. We compute the normalized scattering representation of fractional Brownian motions, which are the only self-similar Gaussian processes with stationary increments. A fractional Brownian motion of Hurst exponent $0 < H < 1$ is defined as a zero mean Gaussian process $\{X(t)\}$, satisfying

$$\forall t, s > 0, \quad \mathbf{E}(X(t)X(s)) = \frac{1}{2}(t^{2H} + s^{2H} - |t - s|^{2H})\mathbf{E}(X(1)^2).$$

It is self-similar and satisfies

$$\forall s > 0, \quad \{X(st)\}_t \stackrel{d}{=} s^H \{X(t)\}_t.$$

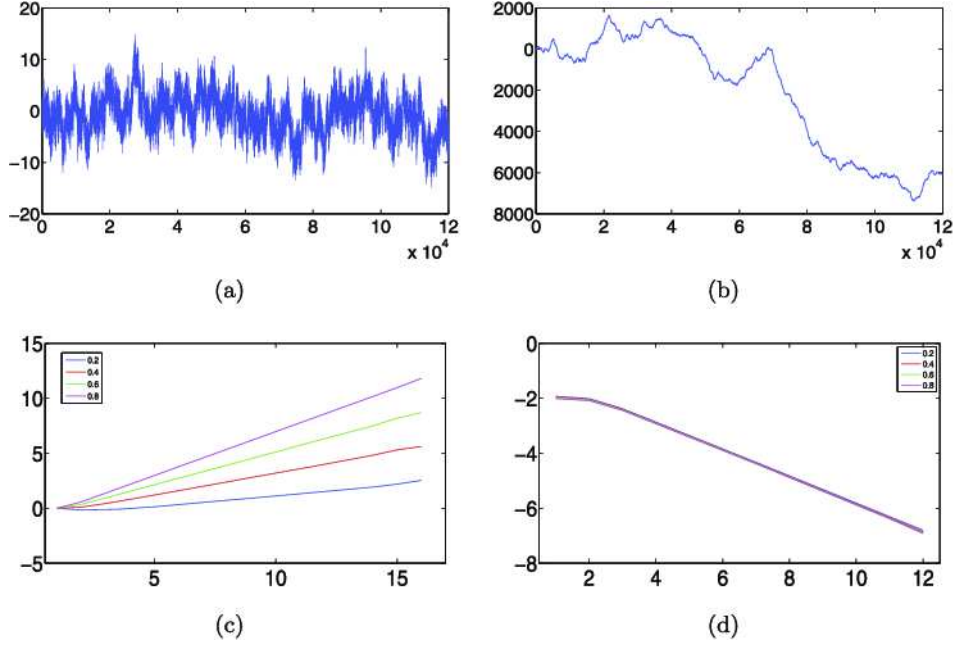


FIG. 3. (a), (b) Realizations of fractional Brownian motions $X(t)$ with $H = 0.2$ in (a) and $H = 0.8$ in (b). (c) $\log_2 \tilde{S}X(j_1)$ as a function of j_1 , for $H = 0.2, 0.4, 0.6, 0.8$. Slopes are equal to H . (d) $\log_2 \tilde{S}X(j_1, j_1 + l)$ as a function of l do not depend on j_1 for all H .

Proposition 3.1 proves in (15) that $\tilde{S}X(j_1) = 2^{Hj_1}$. This is verified by Figure 3(a) which shows that $\log_2 \tilde{S}X(j_1) = Hj_1$ for several fractional Brownian motions with $H = 0.2, 0.4, 0.6, 0.8$.

Figure 3(c) displays $\log_2 \tilde{S}(j_1, j_2)$, which is a function of $j_2 - j_1$, as proved by (16). Modulo a proper initialization at $t = 0$, if X is a fractional Brownian motion of exponent H then $d^\alpha X$ is a fractional Brownian motion of exponent $H - \alpha$. We thus expect from (9) that $\log_2 \tilde{S}X(j_2 - j_1)$ nearly does not depend upon H . This is shown by Figure 3(c) where all curve superimpose for $j_2 - j_1 > 0$, with a slope of $-1/2$. This result is proved by the following theorem.

THEOREM 3.2. *Let $X(t)$ be a fractional Brownian motion with Hurst exponent $0 < H < 1$. There exists a constant $C > 0$ such that for all $j_1 \in \mathbb{Z}$*

$$(19) \quad \lim_{l \rightarrow \infty} 2^{l/2} \tilde{S}X(j_1, j_1 + l) = C.$$

For a fractional Brownian motion, $\log_2 \tilde{S}X(j_1, j_1 + l)$ does not depend on j_1 or H , and its slope is thus equal to $-1/2$ when l increases. This value is characteristic of wide-band Gaussian stationary processes. It indicates that there is no intermittency phenomenon at any scale.

3.3. α -stable Lévy processes. In this section, we compute the scattering moments of α -stable Lévy processes and analyze their intermittency behavior for $1 < \alpha \leq 2$. These processes have finite polynomial moments only for degree strictly smaller than $\alpha \leq 2$ [23]. Indeed, for $\alpha > 1$, α -stable Lévy process $X(t)$ have stationary increments and $\mathbf{E}(|X(t) - X(t - \tau)|) < \infty$ for any $\tau \in \mathbb{R}$. Its scattering moments are thus well defined at all orders. Self-similar Lévy processes have stationary increments with heavy tailed distributions. Their realizations contain rare, large jumps, which are responsible for the blow up of moments larger than α . They induce a strongly intermittency behavior.

$X(t)$ satisfies the self-similarity relation

$$(20) \quad \{X(st)\}_t \stackrel{d}{=} s^{\alpha-1} \{X(t)\}_t,$$

so Proposition 3.1 proves that

$$(21) \quad \tilde{S}X(j_1) = 2^{j_1 \alpha^{-1}}.$$

This is verified in Figure 4 which shows that $\log_2 \tilde{S}X(j_1) = \alpha^{-1} j_1$. First-order moments thus do not differentiate a Lévy stable processes from fractional Brownian motions of Hurst exponent $H = \alpha^{-1}$.

The self-similarity implies that $\tilde{S}X(j_1, j_1 + l)$ does not depend on j_1 . However, they have a very different behavior than second-order scattering moments of fractional Brownian motion. Figure 4 shows that $\log_2 \tilde{S}X(j)$ has a slope which tends to $\alpha^{-1} - 1$ and hence that when l increases

$$(22) \quad \tilde{S}X(j_1, j_1 + l) \simeq 2^{l(\alpha^{-1}-1)}.$$

For $\alpha < 2$, then $\alpha^{-1} - 1 > -1/2$, so $\tilde{S}X(j_1, j_1 + l)$ has a slower decay for α -stable Lévy processes than for fractional Brownian motion, which corresponds to the fact that these processes are highly intermittent and the intermittency increases when α decreases. For $\alpha = 2$, the Lévy process X is a Brownian motion and we recover that $\tilde{S}X(j_1, j_1 + l) \simeq 2^{-l/2}$ as proved in Theorem 3.2.

The scaling property (22) is explained qualitatively, without formal proof. We proved in (16) that

$$(23) \quad \tilde{S}X(j_1, j_2) = \frac{\mathbf{E}(|X \star \psi(t)| \star \psi_l)}{\mathbf{E}(|X \star \psi|)} \quad \text{for } l = j_2 - j_1.$$

The stationary process $|X \star \psi(t)|$ measures the amplitude of local variations of the process X . It is dominated by a sparse sum of large amplitude bumps of the form $a|\psi(t - u)|$, where a and u are the random amplitudes and positions of rare large amplitude jumps in $X(t)$, distributed according to the Lévy measure. It results that

$$(24) \quad \mathbf{E}(|X \star \psi| \star \psi_l) \simeq \mathbf{E}(|dX \star \bar{\psi}| \star \psi_l) \quad \text{with } \bar{\psi}(t) = \int_0^t \psi(u) du.$$

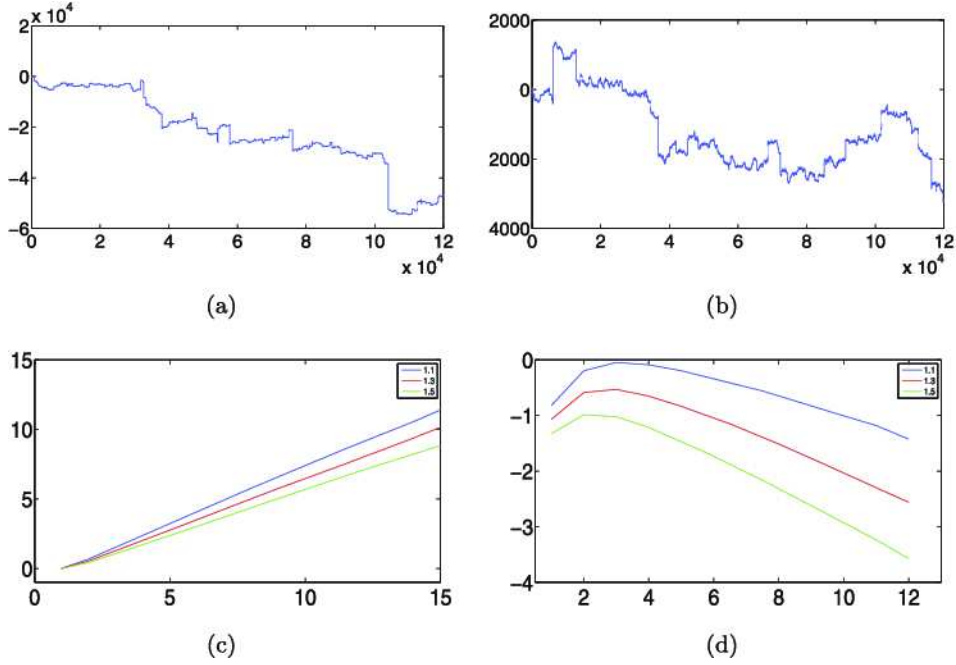


FIG. 4. (a), (b) Realizations of α -stable Lévy processes $X(t)$ with $\alpha = 1.1$ and $\alpha = 1.5$. (c) $\log_2 \tilde{S}X_\alpha(j_1)$ as a function of j_1 with $\alpha = 1.1, 1.2, 1.3$. Slopes are equal to α^{-1} . (d) $\log_2 \tilde{S}X_\alpha(j_1, j_1 + l)$ as a function of l do not depend on j_1 . Slopes tend to $\alpha^{-1} - 1$ when l increases.

If $2^l \gg 1$, then $|\bar{\psi}| \star \psi_l \approx \|\bar{\psi}\|_1 \psi_l$, and $\mathbf{E}(|dX \star \psi_l|) \simeq 2^{l(\alpha^{-1}-1)}$ because the Lévy measure $dX(t)$ satisfies the self-similarity property

$$\{dX(st)\}_t \stackrel{d}{=} s^{\alpha^{-1}-1} \{dX(t)\}_t.$$

Inserting (24) in (23) gives the scaling property (22).

4. Scattering moments of multiplicative cascades. We study the scattering representation of multifractal processes which satisfy a stochastic scale invariance property. Section 4.2 studies the particularly important case of log-infinitely divisible multiplicative processes.

4.1. *Stochastic self-similar processes.* We consider processes with stationary increments which satisfy the following stochastic self-similarity:

$$(25) \quad \forall 1 \geq s > 0, \quad \{X(st)\}_{t \leq 2^L} \stackrel{d}{=} A_s \cdot \{X(t)\}_{t \leq 2^L},$$

where A_s is a log-infinitely divisible random variable independent of $X(t)$ and the so-called *integral scale* 2^L is chosen (for simplicity) as a power of

2. The Multifractal Random Measures (MRM) introduced by [6, 29] are important examples of such processes. Let us point out that MRMs are stationary increments versions of grid bound multiplicative cascades initially introduced by Yaglom [38] and Mandelbrot [26, 27], and further studied by Kahane and Peyriere [22]. In that respect, all the results that we obtain on MRMs can be easily generalized to discrete multiplicative cascades. For the sake of conciseness, we did not include them here.

Since X has stationary increments and satisfies (25), with a change of variables, we verify that $\forall j \leq L$, $\{X \star \psi_j(t)\}_t \stackrel{d}{=} A_{2^j} \{X \star \psi(2^{-j}t)\}_t$, and hence, for all $q \in \mathbb{Z}$ and $j \leq L$

$$(26) \quad \mathbf{E}(|X \star \psi_j|^q) = \mathbf{E}(|A_{2^j}|^q) \mathbf{E}\{|X \star \psi|^q\} \simeq C_q 2^{j\zeta(q)},$$

where $\zeta(q)$ is a priori a nonlinear concave function of q [17, 18]. Similarly to Proposition 3.1, the following proposition shows that normalized scattering moments capture stochastic self-similarity with a univariate function.

PROPOSITION 4.1. *If X is randomly self-similar in the sense of (25) with stationary increments, then for all $j_1 \leq L$*

$$(27) \quad \tilde{S}X(j_1) = \mathbf{E}(|A_{2^{j_1}}|).$$

Moreover, if $2^{j_1} + 2^{j_2} \leq L$ then

$$(28) \quad \tilde{S}X(j_1, j_2) = \overline{S} \tilde{X}(j_2 - j_1) \quad \text{with} \quad \tilde{X}(t) = \frac{|X \star \psi(t)|}{\mathbf{E}(|X \star \psi|)}.$$

PROOF. Property (15) is a particular case of (26) for $q = 1$. If $j_1 + j_2 \leq L$, with the same derivations as for (18), we derive from (25) that

$$(29) \quad ||X \star \psi_{j_1}| \star \psi_{j_2}| \stackrel{d}{=} A_{2^{j_1}} L_{j_1} |X \star \psi| \star \psi_{j_2 - j_1}|,$$

so $\overline{S}X(j_1, j_2) = \mathbf{E}(A_{2^{j_1}}) \mathbf{E}(|X \star \psi| \star \psi_{j_2 - j_1}|)$. Together with (27), it proves (28). \square

Figure 5 shows the normalized scattering of a multiplicative cascade process described in Section 4.2, with an integral scale $2^L = 2^{17}$. When $2^{j_2} \geq 2^L$ is beyond the integral scale, as for a Poisson process, wavelet coefficients converge to Gaussian processes. It results that $\log_2 \tilde{S}(j_1, j_2)$ decays with a slope $-1/2$ as a function of $j_2 - j_1$ for $j_2 > L$, as shown in Figure 5(a). If $j_1 < j_2 < L$ then (28) proves that $\tilde{S}X(j_1, j_2)$ only depends on $j_2 - j_1$, and all curves in Figure 5(b) superimpose in this range.

Propositions 3.1 and 4.1 show that the stationary property $\tilde{S}X(j_1, j_2) = \tilde{S}X(j_2 - j_1)$ can be used to detect the presence of self-similarity, both deterministic and stochastic. This necessary condition is an alternative to the scaling of the q -order moments, $\mathbf{E}(|X \star \psi_j|^q) \simeq C_q 2^{j\zeta(q)}$, which is difficult to verify empirically for $q \geq 2$ or $q < 0$.

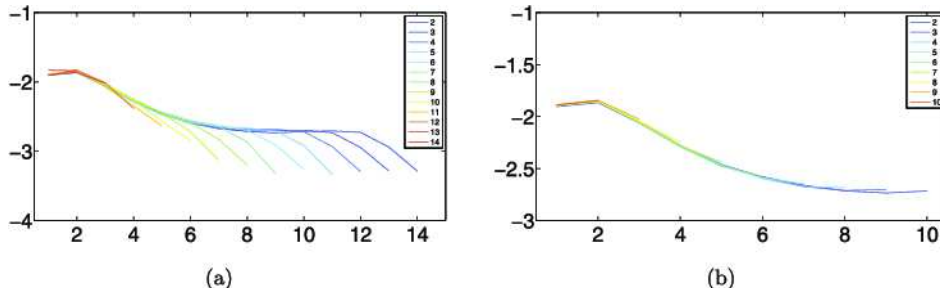


FIG. 5. (a) $\log_2 \overline{S}X_\alpha(j_1, j_1 + l)$ as a function of l for a Multifractal Random Measure (MRM) with $\lambda^2 = 0.04$ and an integral scale $2^L = 2^{13}$. Different colors stand for different values of j_1 . (b) Same curves restricted to $j_2 = j_1 + l < L - 1$.

4.2. *Log-infinitely divisible Multifractal Random Processes.* Multiplicative cascades as introduced by Mandelbrot in [26, 27] are built as an iterative process starting at scale 2^L . They are obtained as the (weak) limit of the measure dM_n whose restriction over a dyadic interval of the form $[k2^{L-n}, (k+1)2^{L-n}]$ is uniform and equal to $\prod_{i=1}^n W_i^{(k)} dt$, where the $W_i^{(k)}$'s are i.i.d. log-infinitely divisible random variables. Multifractal Random Measures (MRM), introduced in [6, 29], are the stationary increments versions of these multiplicative cascades, and are an important class of processes reproducing multi-fractal behavior while having stationary increments. They are built using an infinitely divisible random noise dP distributed in the half-plane (t, s) ($s > 0$). Using the previous notations, the noise around (t, s) can be seen as the equivalent of the infinitely divisible variable $\log_2 W_{\log s}^{(t/s)}$. More precisely, if $\omega_l^{2^L}(t) = \int_{\mathcal{A}_l^{2^L}(t)} dP$ where $\mathcal{A}_l^{2^L}(t)$ is the cone in the (t, s) half-plane pointing to point $(t, 0)$ and truncated for $s < l$, the MRM is defined as the weak limit: $dM(t) = \lim_{l \rightarrow 0} e^{\omega_l^{2^L}(t)} dt$. For a rigorous definition of $\omega_l^{2^L}$ and of a Multifractal Random Measure, we refer the reader to [6].

One can prove that dM satisfies (25), and hence that is multifractal, in the sense that

$$\mathbf{E}(|X \star \psi_j|^q) = \mathbf{E}(|A_{2^j}|^q) \mathbf{E}\{|X \star \psi|^q\} \simeq C_q 2^{j\zeta(q)},$$

where $\zeta(q)$ is a nonlinear function which is uniquely defined by the infinitely divisible law chosen for dP . If dP is Gaussian, dM is generally referred to as a “log-Normal” MRM, and in this case [6]:

$$(30) \quad \zeta(q) = \left(1 + \frac{\lambda^2}{2}\right)q - \frac{\lambda^2}{2}q^2.$$

The curvature of the concave function $\zeta(q)$ at $q = 0$ (λ^2 in the latter case) plays the role of the so-called “intermittency factor” in the multifractal formalism [17, 18]. The larger λ^2 , the more intermittency.

The self-similarity properties of dM are mainly direct consequences of the “global” self-similarity properties of $\omega_l^{2^L}$:

$$(31) \quad \{\omega_{sl}^{s2^L}(st)\}_t \stackrel{\text{law}}{=} \{\omega_l^{2^L}(t)\}_t, \quad \forall L, \forall s > 0,$$

and of the stochastic self-similarity property:

$$(32) \quad \{\omega_{sl}^{2^L}(su)\}_{u < T} \stackrel{\text{law}}{=} \{\Omega_s + \omega_l^{2^L}(u)\}_{u < T}, \quad \forall L, \forall s < 1,$$

where Ω_s is an infinitely divisible random variable independent of $\omega_l^{2^L}(u)$ such that $E(e^{q\Omega_s}) = e^{-(q-\zeta(q))\ln(s)}$. More precise results used in the proofs are stated in Appendix D in [10].

In this section, we will study the scaling properties of scattering moments associated with $X = dM$. Thanks to the discussion in Section 2.3, one can easily show that all our results can be extended to $X(t) = M(t) = \int_0^t dM$. The following theorem characterizes the behavior of normalized first- and second-order scattering moments of dM :

THEOREM 4.2. *Let dM be a Multifractal Random Measure, then*

$$(33) \quad \forall j < L, \quad \tilde{S} dM(j) = 1,$$

and if $\zeta(2) > 1$ then as long as $j_1, j_2 < L$, $\tilde{S} dM(j_1, j_2)$ depends only on $j_1 - j_2$ and there exists $\tilde{K} > 0$ such that for each $j_2 \leq L$

$$(34) \quad \lim_{j_1 \rightarrow -\infty} \tilde{S} dM(j_1, j_2) = \tilde{K}.$$

The proof is in Appendix E in [10]. Let us illustrate this theorem in the log-normal case. Figures 6(a), (b) displays two realizations of log-Normal MRM cascades for $\lambda^2 = 0.04$ and $\lambda^2 = 0.07$, with an integral scale $2^L = 2^{13}$. Figure 6(c) shows estimations of normalized first-order scattering moments for $\lambda^2 = 0.04$, $\lambda^2 = 0.07$ and $\lambda^2 = 0.1$. As predicted by Theorem 4.2, $\log_2 \tilde{S} dM(j_1) = 0$ for $j_1 < L = 13$. The second-order scattering moments for the same values of λ^2 are displayed in Figure 6(d). As expected from Theorem 4.2, $\log_2 \tilde{S} dM(j_1, j_2)$ only depends on $j_2 - j_1$ for $j_2 < L$. It converges to a constant \tilde{K} when $j_2 - j_1$ increases.

With a Taylor expansion, one can show that, for large $j_2 - j_1$, \tilde{K} is a linear function of λ up to some $O(\lambda^2)$ additive term. This is numerically verified by Monte Carlo simulations which shows that $\tilde{K} \approx 0.82\lambda$. We see here again the correspondence between scattering coefficients and intermittency measurements. The constant 0.82 depends upon the choice of wavelet ψ .

Another important class of stochastic self-similar processes are the Multifractal Random Walks (MRW) [6, 31], defined as $X(t) = B(M(t))$, where

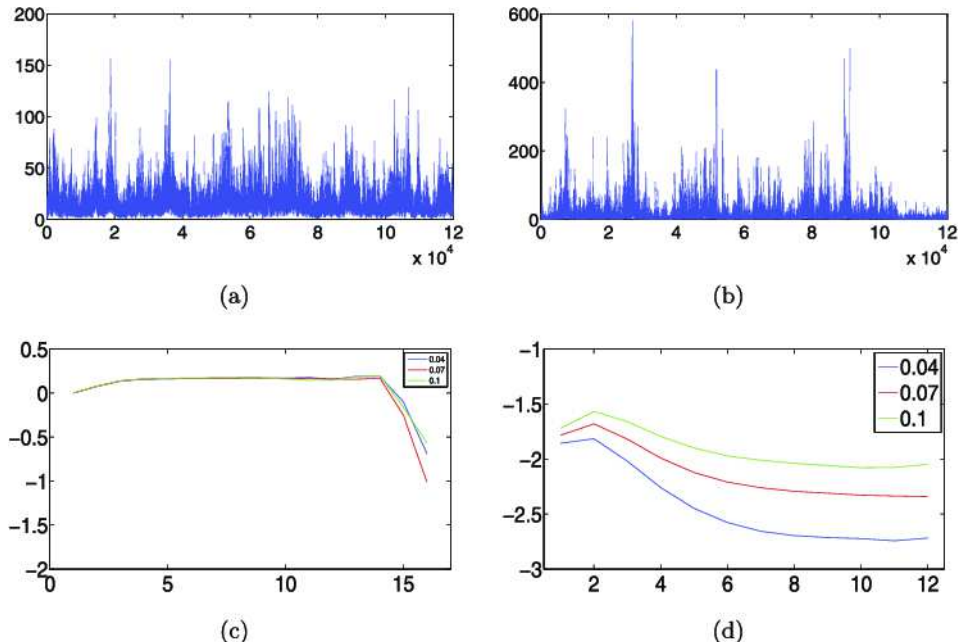


FIG. 6. (a), (b) Realizations dM of log-normal Multifractal Random Measures with $\lambda^2 = 0.04$ and $\lambda^2 = 0.1$. (c) $\log_2 \tilde{S} dM(j_1)$ with $\lambda^2 = 0.04$, $\lambda^2 = 0.07$ and $\lambda^2 = 0.1$. (d) $\log_2 \tilde{S} dM(j_1, j_1 + l)$, for $\lambda^2 = 0.04$, $\lambda^2 = 0.07$ and $\lambda^2 = 0.1$, as a function of l , for $j_1 + l < L$ where $2^L = 2^{13}$ is the integral scale.

$B(t)$ is a standard Brownian motion and $M(t)$ is an MRM. MRWs are stochastic volatility models, which account for asset price fluctuations in financial markets by mimicking the stochastic behavior of asset volatility [4, 5, 31]. Appendix F in [10] shows that the MRW satisfies the analog of Theorem 4.2, with the same second-order behavior, revealing the underlying intermittency structure introduced by $M(t)$, but different first-order asymptotics, due to the scaling of the Brownian motion.

5. Parametric model estimation with scattering moments. Section 5.1 introduces estimators of scattering moments. Section 5.2 applies the generalized method of simulated moments to estimate the parameters of data generating models. Sections 5.5 and 5.6 analyze the scattering moments of turbulence data and financial time series to evaluate fractional Brownian, Lévy stable and multifractal cascade models.

5.1. *Estimation of scattering moments.* We study scattering moment estimators introduced in [25], and compute upper bounds of their mean-square error. A scattering moment $\overline{S}X(j_1, \dots, j_m) = \mathbf{E}(|X \star \psi_{j_1} | \star \dots \star \psi_{j_m}|)$ is estimated by replacing the expected value by a time averaging at a scale 2^M .

It is calculated with a time window $\phi_M(t) = 2^{-M}\phi(2^{-M}t)$ with $\int \phi(t) dt = 1$. For any $(j_1, \dots, j_m) \in \mathbb{Z}^m$ with $j_k \leq M$, the estimator is

$$(35) \quad \widehat{S}X(j_1, \dots, j_m) = ||X \star \psi_{j_1} | \star \dots | \star \psi_{j_m} | \star \phi_M(t_0),$$

where t_0 is typically in the middle of the domain where $X(t)$ is known. Since $\int \phi_M(t) dt = 1$, this estimator is unbiased $\mathbf{E}(\widehat{S}X(j_1, \dots, j_m)) = \overline{S}X(j_1, \dots, j_m)$. The following theorem, proved in Appendix G in [10], gives an upper bound of the mean squared estimation error at each scale.

THEOREM 5.1. *Suppose that the Fourier transform $\Phi(\omega)$ of ϕ satisfies*

$$(36) \quad |\Phi(\omega)|^2 \leq \frac{1}{2} \sum_{j=1}^{\infty} (|\Psi(2^j \omega)|^2 + |\Psi(-2^j \omega)|^2) \quad \text{with } \Phi(0) = 1.$$

If X has stationary increments and $\mathbf{E}(|X \star \psi_{j_1}|^2) < \infty$ then the mean squared estimation error

$$\begin{aligned} \varepsilon(j_1) &\stackrel{\text{def}}{=} \mathbf{E}(|\widehat{S}X(j_1) - \overline{S}X(j_1)|^2) \\ &\quad + \sum_{m=2}^{\infty} \sum_{-\infty < j_2, \dots, j_m \leq M} \mathbf{E}(|\widehat{S}X(j_1, \dots, j_m) - \overline{S}X(j_1, \dots, j_m)|^2) \end{aligned}$$

satisfies

$$(37) \quad \varepsilon(j_1) \leq \sigma^2(|X \star \psi_{j_1}|) - \sum_{m=2}^{\infty} \sum_{-\infty < j_2, \dots, j_m \leq M} |\overline{S}X(j_1, \dots, j_m)|^2.$$

When j_1 is close to M then $|X \star \psi_{j_1}(t)|$ decorrelates slowly relatively to the averaging window scale 2^M so $\varepsilon(j_1)$ is large, but it is bounded by $\sigma^2(|X \star \psi_{j_1}|)$. Large variance estimators $\widehat{S}X(j_1, \dots, j_m)$ are eliminated by keeping only small scales $j_k \leq J$ for $1 \leq k \leq m$, with $M - J$ sufficiently large. For most classes of random processes, including fractional Brownian motions and multi-fractal random walks, we observe numerically that $\varepsilon(j_1)$ converges to zero as the averaging scale 2^M goes to ∞ . Equation (37) proves that it is the case if for all j_1

$$\sigma^2(|X \star \psi_{j_1}|) = \sum_{m=2}^{\infty} \sum_{-\infty < j_2, \dots, j_m \leq \infty} |\overline{S}X(j_1, \dots, j_m)|^2.$$

This energy conservation has been conjectured for large classes of processes in [25], but it is not proved.

For n independent realizations $\{X_k(t)\}_{1 \leq k \leq n}$, we compute an averaged scattering estimator

$$(38) \quad \widehat{S}X = n^{-1} \sum_{k=1}^n \widehat{S}X_k.$$

Its variance is thus reduced by n^{-1} . When n goes to ∞ , the central limit theorem proves that $\widehat{S}X - \overline{S}X$ converges to a zero-mean normal distribution whose variance goes to 0.

5.2. *Generalized method of simulated scattering moments.* The generalized method of simulated moments [28] computes parameter estimators for data generative models, from arbitrary families of moments. We apply it to scattering moments.

Suppose that $\{X_k\}_{1 \leq k \leq n}$ are n independent realizations of a parametric model Y_θ . Then $\widehat{S}X$ is an unbiased estimator of $\overline{S}Y_\theta$, so $m(\theta) = \mathbf{E}(\widehat{S}X) - \overline{S}Y_\theta = 0$. The generalized method of moments estimates this moment condition with

$$(39) \quad \hat{m}(\theta) = \widehat{S}X - \overline{S}Y_\theta.$$

When n goes to ∞ the central limit theorem proves that $\hat{m}(\theta)$ converges to a normal distribution. The generalized method of moments finds the parameter $\hat{\theta}$ such that $\hat{\theta} = \operatorname{argmin}_\theta \hat{m}(\theta)W\hat{m}(\theta)^T$ for appropriate matrices W . Setting $W = Id$ gives

$$(40) \quad \hat{\theta}_1 = \operatorname{argmin}_\theta \|\widehat{S}X - \overline{S}Y_\theta\|^2.$$

The two-step generalized method of moment updates the first estimator $\hat{\theta}_1$ by setting $W = \widehat{W}_{\hat{\theta}_1}$, where \widehat{W}_θ is the inverse of the empirical covariance

$$(41) \quad \widehat{W}_\theta = \left(n^{-1} \sum_{k=1}^n (\widehat{S}X_k - \overline{S}Y_\theta)(\widehat{S}X_k - \overline{S}Y_\theta)^T \right)^{-1}.$$

It computes

$$(42) \quad \hat{\theta} = \operatorname{argmin}_\theta \hat{m}(\theta)\widehat{W}_{\hat{\theta}_1}\hat{m}(\theta)^T.$$

Since in general we cannot compute $\overline{S}Y_\theta$ analytically, according to the simulated method of moments [28], $\overline{S}Y_\theta$ is replaced in (39) and (41) by an estimator $\widehat{S}Y_\theta$ calculated with a Monte Carlo simulation. This estimator is computed with $n' \gg n$ realizations which are adjusted in order to yield a negligible mean-square error $\mathbf{E}(\|\widehat{S}Y_\theta - \overline{S}Y_\theta\|^2)$. We also compute a p -value for the null hypothesis which supposes that the parameterized model is valid. The J-test [16] is a chi-squared goodness of fit test normalized by the $p - d$ degrees of freedom:

$$(43) \quad \chi_{\text{red}}^2 = (p - d)^{-1} n \hat{m}(\hat{\theta})\widehat{W}_{\hat{\theta}_1}\hat{m}(\hat{\theta})^T.$$

Under the null hypothesis, $(p - d)\chi_{\text{red}}^2$ asymptotically follows a chi-squared distribution with $p - d$ degrees of freedom.

In practice, one must optimize the number p of scattering moments to have enough discriminability with an estimator having small variance. In the present work, we limit ourselves to first- and second-order scattering:

$$\overline{S}X = (\overline{S}X(j_1), \overline{S}X(j_1, j_2))_{J_0 < j_1 \leq J, j_1 < j_2 \leq J}.$$

Indeed, finest scale coefficients $j_1 \leq J_0$ are removed to avoid errors due to aliasing, discretization or to some data smoothing. Similarly, large scale coefficients $j_i > J$ are also removed to since to the largest variance estimators, and $\overline{S}X(j_1, j_2)$ for $j_2 \leq j_1$ are also eliminated because they carry little information on X . The resulting scattering vector has $J - J_0$ first-order scattering moments and $(J - J_0 - 1)(J - J_0)/2$ second-order moments.

If we observe a single realization $X(t)$ where sufficiently far away wavelet coefficients become independent, $\widehat{S}X$ becomes asymptotically normal when computed at intervals Δ :

$$(44) \quad \begin{aligned} \widehat{S}X_k(j_1) &= |X \star \psi_{j_1}| \star \phi_M(k\Delta) \quad \text{and} \\ \widehat{S}X_k(j_1, j_2) &= ||X \star \psi_{j_1}| \star \psi_{j_2}| \star \phi_M(k\Delta). \end{aligned}$$

The goodness of fit J-test supposes that the variable (43) follows a chi-squared distribution with $p - d$ degrees of freedom, which requires that the estimators $\widehat{S}X_k$ are independent for different k . If X has an integral scale T , as in multifractal cascades, then increments are independent at distances larger than T . One can thus set $\Delta = 2T$. Other processes, such as fractional Brownian motions have no integral scales but their wavelet coefficients become nearly independent at distances much larger than the scale. Nearly independent estimators are thus obtained if $\Delta \gg 2^M$.

The situation is easier if we are only interested in the parameter estimator $\hat{\theta}$ with (42), without goodness of fit. Its consistency requires that $\widehat{S}X$ converges to a normal distribution, but we can estimate its covariance up to an unknown multiplicative factor. Thus, setting $\Delta = 1$ only introduces a multiplicative factor in the covariance estimation, which does not affect the estimator $\hat{\theta}$ in (42).

5.3. *Intermittency estimation on multiplicative cascades.* The properties of the Scattering Method of Moments are illustrated on the estimation of the intermittency parameter $\theta = \lambda^2$ for multifractal random measures. Section 4.2 proves that normalized second-order scattering moments converge to a constant \tilde{K} which is proportional to λ , showing that the intermittency λ^2 is characterized by first- and second-order scattering moments. However, the information is not just carried by this asymptotic value, which is why all scattering moments are used for the estimation. The scattering estimation is compared with two estimators dedicated to this particular estimation problem [5].

TABLE 1

Estimation of λ^2 for a multi-fractal random measure. The table gives the mean and the standard deviation of estimators computed with a wavelet moment regressions (45), a log covariance regression (46), and the method of simulated scattering moments, for several values of λ^2 and several sample sizes N

λ^2	N	$\hat{\theta}$ wavelet	$\hat{\theta}$ log-cov	$\hat{\theta}$ scattering	J	χ_{red}^2	p -value
0.02	10^6	$0.025 \pm 2 \cdot 10^{-3}$	$0.02 \pm 2 \cdot 10^{-4}$	$0.02 \pm 2 \cdot 10^{-4}$	7	1.1 ± 0.3	0.7 ± 0.3
0.05	10^6	$0.055 \pm 2 \cdot 10^{-3}$	$0.05 \pm 6 \cdot 10^{-4}$	$0.05 \pm 3 \cdot 10^{-4}$	6	0.8 ± 0.3	0.5 ± 0.3
0.1	10^6	$0.105 \pm 4 \cdot 10^{-3}$	0.1 ± 10^{-3}	0.1 ± 10^{-3}	5	0.8 ± 0.5	0.5 ± 0.3
0.1	10^5	0.109 ± 10^{-2}	$0.1 \pm 3 \cdot 10^{-3}$	$0.1 \pm 2 \cdot 10^{-3}$	5	0.7 ± 0.3	0.3 ± 0.3
0.1	10^4	$0.12 \pm 3 \cdot 10^{-2}$	$0.1 \pm 1.3 \cdot 10^{-2}$	$0.1 \pm 9 \cdot 10^{-3}$	5	N/A	N/A

Scattering moment estimators are computed from n independent realizations of size 2^{11} of a multifractal random measure having an integral scale $T = 2^{10}$. The total number of data points is $N = n \cdot 2^{11}$, and we set $J_0 = 0$. For different values of $N = n \cdot 2^{11}$, we report in Table 1 the value of J which minimizes the mean squared error $\mathbf{E}(|\hat{\theta} - \theta|^2)$, estimated with Monte Carlo simulations. We also give the average value of the reduced χ_{red}^2 test in (43) and the model p -value. For small values of n , the covariance of $\hat{S}X$ is computed up to a multiplicative constant, from correlated scattering coefficients calculated within each realization with $\Delta = 1$ in (44). It leads to a good estimation of $\hat{\theta}$ but the model p -value cannot be estimated.

The intermittency parameter of multifractal random measures can also be estimated directly from wavelet coefficients. Section 4.2 explains that the scaling exponent of wavelet moments of order q is $\zeta(q) = (\frac{1}{2} + \lambda^2)q - \frac{\lambda^2}{2}q^2$. It results that $\lambda^2 = 2\zeta(1) - \zeta(2)$. The intermittency parameter can thus be estimated with a linear regression on the estimated first- and second-order moments of wavelet coefficients at scales $2^j < 2^L$:

$$(45) \quad 2 \log_2 \mathbf{E}(|X \star \psi_j|^2) - \log_2 \mathbf{E}(|X \star \psi_j|)^2 \approx j(\zeta(2) - 2\zeta(1)) + C.$$

The wavelet moments $\mathbf{E}(|X \star \psi_j|^2)$ and $\mathbf{E}(|X \star \psi_j|)$ are estimated with empirical averages of $|X \star \psi_j|$ and $|X \star \psi_j|^2$, calculated from the N data samples. An improved estimator has been introduced in [4, 5] with a regression on the covariance of the log of the multifractal random measure. One can indeed prove that

$$(46) \quad \text{Cov}(\log|X \star \psi_j(t)|, \log|X \star \psi_j(t+l)|) \simeq -\lambda^2 \ln\left(\frac{l}{2^L}\right) + o\left(\frac{j}{l}\right),$$

which leads to lower variance estimations.

Table 1 shows that the scattering moment estimation of λ^2 has a smaller variance than the regression of first- and second-order wavelet moments.

This is due to the low variance of the scattering estimators which are computed with nonexpansive operators. It gives comparable results with the log-covariance estimator, which was optimized for this problem [5], and which is also closely related to the wavelet leaders estimator of [20]. In the case of log-normal multiplicative cascades, the log-covariance estimator does not suffer from outliers, although it is not a contractive operator, and the log-log linear regression used to recover $\hat{\lambda}^2$ in (46) reduces the variance of the estimator. This explains the similar behavior with respect to the GMM scattering estimator.

The J-test validates the multifractal model, since we obtain a normalized J-test with mean and standard deviation close to $1 \pm \sqrt{\frac{2}{p-1}}$, corresponding to mean and standard deviation of a chi-squared distribution with $p - 1$ degrees of freedom. The resulting p -values for rejecting the true model are of the order of 0.5. As expected, reducing the maximum scattering scale J improves the estimation of λ^2 for high intermittencies. It removes large variance coefficients. However, numerical experiments confirm that the generalized method of moments is robust to the choice of J , because the inverse covariance \widehat{W} in (42) reduces the impact of high variance coefficients.

5.4. *Estimation of Blumenthal–Gethoor index on Lévy processes.* We apply the same methodology to estimate the Blumenthal–Gethoor index of Lévy processes, defined as

$$\beta = \inf \left\{ r \geq 0 \text{ s.t. } \int_{|x| \leq 1} |x|^r d\Pi(x) < \infty \right\},$$

where $\Pi(x)$ is the Lévy measure associated to an observed Lévy process $X(t)$. If $X(t)$ is α -stable, then $\beta = \alpha$. This index can be estimated using spectral methods in [8], which require an estimation of the characteristic function.

We concentrate in the case of α -stable processes, and we assume here that $1 < \alpha \leq 2$, which implies that we cannot consider the covariance of $\widehat{S}X$. Instead, we use the simplified GMM estimator (40). Besides the simplified GMM scattering estimator, we also consider a log-linear regression on wavelet coefficients

$$\log_2 \mathbf{E}|X \star \psi_j| \simeq \alpha^{-1}j,$$

and also a log-linear regression on scattering moments, using the asymptotic results of Section 3.3:

$$\log_2 SX(j) \simeq \alpha^{-1}j, \quad \log_2 \widetilde{S}X(j_1, j_1 + l) \simeq (\alpha^{-1} - 1)l.$$

For that purpose, we estimate scattering moments $\widehat{S}X(j_1, j_2)$ with $j_2 \geq j_1 + \delta$ and $\delta = 3$. Table 2 shows that a regression on scattering moments improves

TABLE 2

Estimation of α for α -stable Lévy. The table gives the mean and the standard deviation of estimators computed with a wavelet moment regressions (45) and the method of simulated scattering moments, for several values of α for $N = 2^{20}$

α	$\hat{\alpha}$ wavelet regr.	$\hat{\alpha}$ scatt. regr.	$\hat{\alpha}$ scattering GMM	J
1.1	1.2 ± 0.1	$1.2 \pm 8 \cdot 10^{-2}$	$1.1 \pm 4 \cdot 10^{-2}$	7
1.5	$1.55 \pm 7 \cdot 10^{-2}$	$1.51 \pm 6 \cdot 10^{-2}$	$1.5 \pm 2 \cdot 10^{-2}$	5

the performance of wavelet regression, and that GMM scattering significantly improves with respect to the regression method. Second-order scattering coefficients produce statistically significant new information, which improves regression results. Moreover, the information on α is not just contained in the asymptotic regime $j_2 \gg j_1$ but also in the transient regime, which is exploited by the GMM estimator.

5.5. *Turbulence energy dissipation.* Turbulent regimes appear in a wide variety of experimental situations, and are characterized by random fluctuations over a wide range of time and space scales. Making a theory of the famous Richardson “energy cascade” across the inertial range remains one of the main challenges in classical physics [15]. Normalized scattering moments are computed over dissipative measurements of a turbulent gas, to analyze their self-similarity and intermittency properties. This study does not pretend evaluating general turbulence physical models. However, it shows that one can have confident model evaluations from data sets, despite intermittency phenomena.

The data we used has been recorded by the group of B. Castaing in Grenoble in a low temperature gaseous Helium jet in which the Taylor scale-based Reynolds number is $R_\lambda = 703$ [12]. A single probe provides measures of velocity temporal variations at a fixed space location that involve both Lagrangian and Eulerian fluctuations. Figure 7(a) shows a sample of the surrogate dissipation field $X(t)$ as a function of time, estimated from the experimental velocity records.² The Kolmogorov (dissipative) scale η is observed at approximately 2^2 sample points, whereas the integral scale is approximately $2^L = 2^{11}$ sample points.

First-order scattering coefficients are normalized at the finest scale defined by $j_1 = 2$. These coefficients are displayed in Figure 7(b). In the inertial range $2^1 = 2^{j_0} < 2^{j_1} \leq 2^L = 2^{11}$ the scaling law of the exponents is $\tilde{S}X(j_1) \simeq 2^{-0.25j_1}$. If $2^{j_1} \geq 2^L$ then $\tilde{S}X(j_1) \simeq 2^{-j_1/2}$ because the low frequencies of a turbulent flow becomes Gaussian and independent beyond the integral scale.

²One assumes the validity of the Taylor hypothesis [15].

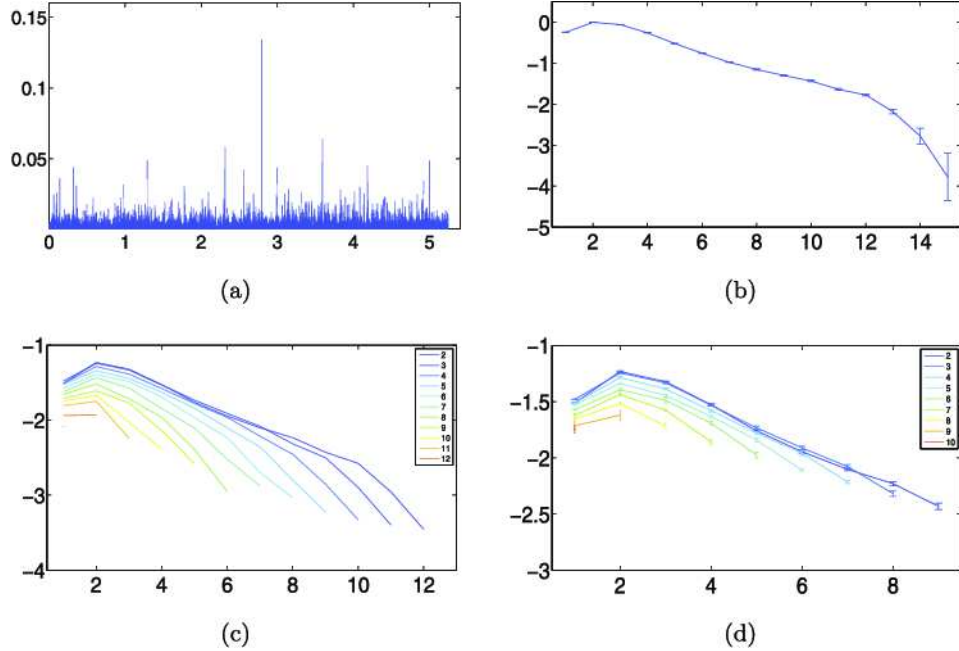


FIG. 7. (a) Realization of dissipation $X(t) = (\frac{\partial v}{\partial t})^2$ in a turbulent flow. (b) Estimation $\log_2 \tilde{S}X(j_1)$ as a function of j_1 , calculated from 4 realizations of 2^{19} samples each. (c) $\log_2 \tilde{S}X(j_1, j_1+l)$ as a function of l , for $2 \leq j_1 \leq 12$. (d) $\log_2 \tilde{S}X(j_1, j_1+l)$ in the inertial range $j_1+l < L-1 = 10$. We plot the confidence intervals corresponding to the standard deviation of the estimated $\log_2 \tilde{S}X(j_1, j_1+l)$.

Figure 7(c) gives estimated normalized second-order coefficients $\log_2 \tilde{S}X(j_1, j_1+l)$ as a function of l , for different j_1 . For $j_2 = j_1+l > L$, the slopes increase up to $-1/2$ because beyond the integral scale, wavelet coefficients converge to Gaussian random processes. Below the integral scale, $j_2 = j_1+l < L-1$, Figure 7(d) shows the curves $\log_2 \tilde{S}X(j_1, j_1+l)$ with error bars giving the standard deviations of each estimated values. In this inertial range, the average slope of all curves is -0.2 . This slope is very different from the $-1/2$ decay of Gaussian processes, which indicate the presence of intermittent phenomena. Although these curves are similar, one can observe that they differ significantly compared to the error bars, which indicates the self-similarity of turbulence data is violated. This nonself-similarity is likely to originate from the fact that, as already observed in [11, 14], Taylor hypothesis does not rigorously hold. We consider the three following models for inertial range turbulence: (i) the square of a Fractional Gaussian Noise parameterized by $\theta = H$, (ii) the square of the increments of α -stable Lévy processes, parameterized by $\theta = \alpha$ and finally (iii) log-normal multifractal random measures, parameterized by the intermittency parameter

TABLE 3
Parameter estimation for the turbulence data in Figure 7(a), calculated from Fractional Brownian Noise measures (FBN), Lévy stable measures (LS), and Multifractal Random Measures (MRM)

	FBN	LS	MRM
$\hat{\theta}$	$H = 0.9$	$\alpha = 1.98$	$\lambda^2 = 0.09$
χ_{red}^2	28	29	29
p -value	$<10^{-6}$	$<10^{-6}$	$<10^{-6}$

$\theta = \lambda^2$. Setting $J_0 = 1$ eliminates coefficients below the diffusion scale. We have $N = 4 \cdot 10^6$ data samples, divided into 4 realizations. Within each realization, since the integral scale is $T = 2 \cdot 10^3$, samples are independent at a distance larger than T . The maximum scale is set to $2^J = 2^8$ but its modification has a marginal impact on the estimation. The size of the resulting scattering vector is $p = (J - J_0 + 1)(J - J_0)/2 = 28$.

Table 3 gives an optimal parameter $\hat{\theta}$ as well as the value of the χ_{red}^2 goodness of fit test in (43), together with its p -value. All models are rejected with very high confidence. For nearly the same number of data values, with integral scales of same size, Table 1 gave much higher p -values for valid multifractal random measure models of same intermittency. Fractional Brownian motions can explain the behavior of first-order scattering, but not the second-order ($-1/2$ as opposed to -0.2). Lévy stable processes have first- and second-order scattering which decay with a slope of $\alpha^{-1} - 1$. To match the slopes in Figure 7(c), (d), respectively equal to -0.25 and -0.2 , we would need that $\alpha \approx 1.2$ which is far from the value $\alpha = 1.98$ obtained in Table 3. Multifractal random measure model misfit comes from their first-order coefficients which remain constant whereas turbulence data coefficients decay with a slope close to -0.2 .

5.6. *Financial time-series analysis.* In the following, we analyze the normalized scattering moments of two financial time series: high-frequency Euro-Bund trade data³ and intraday S&P 100 index trade data. Each trade occurs at a given price, whose logarithm is noted $X(t)$.

Every single day, the logarithmic returns of the price [i.e., the increments of $X(t)$] are computed on rolling 10 second intervals, after preprocessing the microstructure noise using the technique advocated in [33]. Each day corresponds to 9 hours of trading, and hence 3240 increments. Intraday

³Euro-Bund is one of the most actively traded financial asset in the world. It corresponds to a future contract on an interest rate of the Euro-zone.

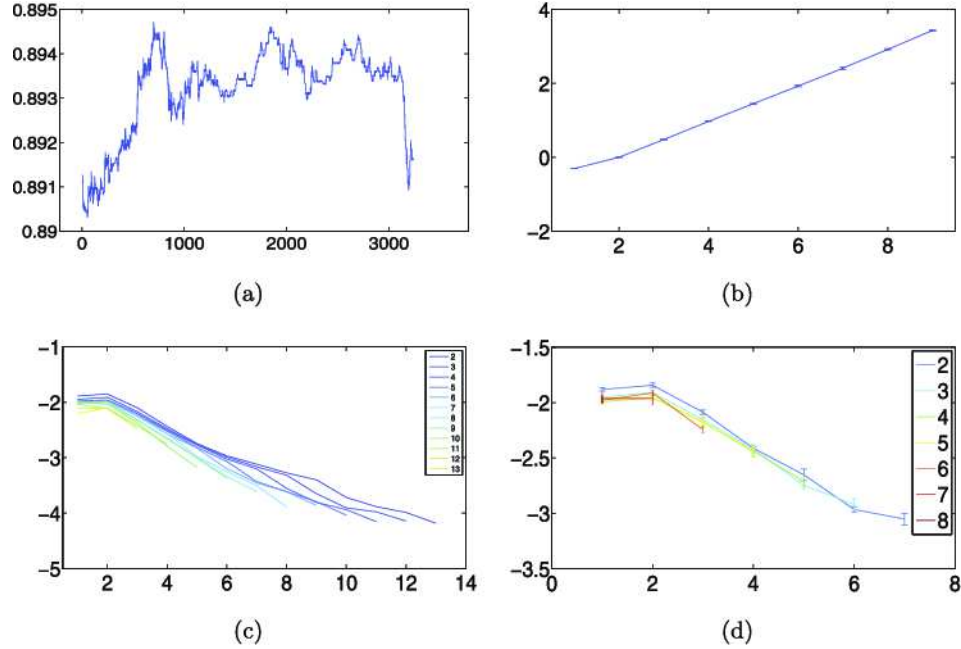


FIG. 8. (a) One day of the deseasonalized Euro-Bund log-price $X(t)$. (b) Estimated $\log_2 \widetilde{S}X(j_1)$. (c) Estimated $\log_2 \widetilde{S}X(j_1, j_1 + l)$. (d) Estimated $\log_2 \widetilde{S}X(j_1, j_1 + l)$ for $j_1 + l < 9$.

financial data are subject to strong seasonal intraday effects. These effects are removed with a standard “deseasonalizing” algorithm which normalizes the returns by the square root of the intraday seasonal variance.

Figure 8 displays the resulting deseasonalized Bund log-price $X(t)$ and its estimated scattering moments. The decay of first-order scattering moments is $\log_2 \widetilde{S}X(j) \sim 0.48j$, whereas for second-order is $\log_2 \widetilde{S}X(j_1, j_1 + l) \sim -0.2l$ for all $j_2 = j_1 + l$. Contrarily to turbulence data, we do not see an integral scale, beyond which second-order coefficients would have a fast decay of $-0.5l$. This is not surprising since the integral scale is known to be larger than few months [5]. Figure 8(d) gives intra-day second-order coefficients $j_2 = j_1 + l < 9$. The variance of $\widetilde{S}X(j_1, j_1 + l)$ is indicated with vertical error bars. Observe that $\log_2 \widetilde{S}X(j_1, j_1 + l)$ has small variations as a function of j_1 , which is a strong indication of self-similarity.

The same scattering computations are performed on the S&P 100 index, sampled every 5 minutes from April 8th, 1997, to December 17th, 2001, to yield 78 samples every day. Figure 9 shows the scattering moments estimated on the S&P time series. Observe that $\log_2 \widetilde{S}X(j_1)$ remains regular for j_1 close to 6, and that for $j_2 = j_1 + l = 6$ the coefficient $\log_2 \widetilde{S}X(j_1, j_1 + l)$ is higher

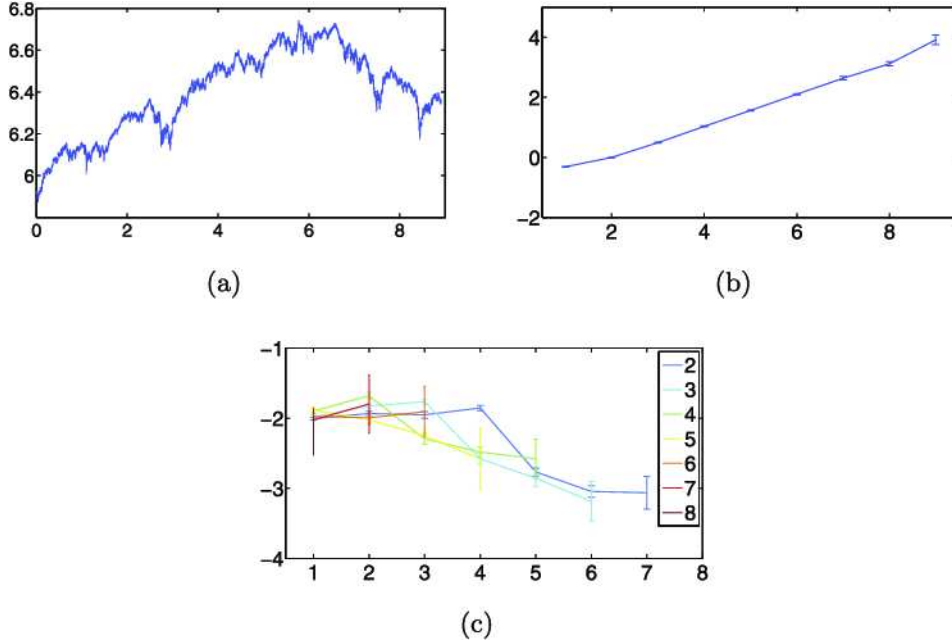


FIG. 9. (a) Three years of the deseasonalized S&P 100 index log-price $X(t)$. (b) Estimated $\log_2 \tilde{S}X(j_1)$. (c) Estimated $\log_2 \tilde{S}X(j_1, j_1 + l)$ for $j_1 + l < 9$.

than expected, relatively to other coefficients, which means a higher level of intermittency. 2^6 roughly corresponds to a trading day $78 \simeq 2^6$.

We consider the three following models: (i) fractional Brownian motions models with $\theta = H$, (ii) Lévy stable processes parameterized with $\theta = \alpha$ and (iii) multifractal random walks with $\theta = \lambda^2$. For each model family, Table 4 estimates an optimal parameter $\hat{\theta}$ from first- and second-order scattering. They are computed from a total of $N = 3 \cdot 10^6$ (resp., $N = 10^5$) samples for the Euro-Bund (resp., S&P 100). The maximum scale 2^J is adjusted to $J = 8$ (resp., $J = 6$), and we set $J_0 = 1$ to eliminate discretization effects in both cases. For fractional Brownian motions, the estimated parameter $\hat{\theta} = H = 0.5$ corresponds to a Brownian motion. Brownian motion models explain the power-spectrum decay of these processes but are known not to be appropriate because they do not take into account the intermittency behavior of financial markets. This appears in the second-order scattering moments of Figure 8(d) and 9(c), which have a much slower decay than Brownian motions. The Lévy-stable parameters α in Table 4 are close to 2 (order 2 moment of financial time-series are known to be finite). Estimated models of multifractal random walks show the existence of intermittency which is larger for the S&P 100 data set than for the Euro-Bund data. For each model, Table 4 gives the value of the J-test variable χ_{red}^2 computed

TABLE 4

The left and right parts of the table correspond to Euro-Bund and S&P 100 time series. The first row gives the estimated parameter value $\hat{\theta}$ for Fractional Brownian Motion (FBM), Lévy stable processes (LS) and Multifractal Random Walks (MRW)

S	Euro-Bund			S&P		
	FBM	LS	MRW	FBM	LS	MRW
$\hat{\theta}$	$H = 0.5$	$\alpha = 1.95$	$\lambda^2 = 0.03$	$H = 0.5$	$\alpha = 1.8$	$\lambda^2 = 0.08$
χ_{red}^2	29	26	23	17	16	10

with (43). Multifractal random walks have the lowest value χ_{red}^2 , and hence provide the better stochastic model of the data. However, one cannot compute a p -value because the empirical covariance matrix is computed from correlated scattering estimators $\widehat{S}X_k$ in (44). Because the integral scale is too large, one cannot fix an interval Δ providing independent scattering values.

SUPPLEMENTARY MATERIAL

Proofs of theorems (DOI: [10.1214/14-AOS1276SUPP](https://doi.org/10.1214/14-AOS1276SUPP); .pdf). We provide the technical derivations of all the results.

REFERENCES

- [1] ABRY, P., FLANDRIN, P., TAQQU, M. S. and VEITCH, D. (2000). Wavelets for the analysis, estimation and synthesis of scaling data. In *Self-Similar Network Traffic and Performance Evaluation* (K. PARK and W. WILLINGER, eds.) 39–88. Wiley, New York.
- [2] ANDEN, J. and MALLAT, S. (2014). Deep scattering spectrum. *IEEE Trans. Signal Process.* **62** 4114–4128.
- [3] ARNEODO, A. and JAFFARD, S. (2004). L’analyse multi-fractale des signaux. *Images des Mathématiques* **2004** 7–14.
- [4] BACRY, E., KOZHEMYAK, A. and MUZY, J.-F. (2008). Continuous cascade models for asset returns. *J. Econom. Dynam. Control* **32** 156–199. [MR2381693](#)
- [5] BACRY, E., KOZHEMYAK, A. and MUZY, J. F. (2013). Log-normal continuous cascade model of asset returns: Aggregation properties and estimation. *Quant. Finance* **13** 795–818. [MR3054792](#)
- [6] BACRY, E. and MUZY, J. F. (2003). Log-infinitely divisible multifractal processes. *Comm. Math. Phys.* **236** 449–475. [MR2021198](#)
- [7] BACRY, E., MUZY, J. F. and ARNEODO, A. (1993). Singularity spectrum of fractal signals from wavelet analysis: Exact results. *J. Stat. Phys.* **70** 635–674. [MR1203712](#)
- [8] BELOMESTNY, D. (2010). Spectral estimation of the fractional order of a Lévy process. *Ann. Statist.* **38** 317–351. [MR2589324](#)
- [9] BRUNA, J. and MALLAT, S. (2013). Invariant scattering convolution networks. *IEEE Transactions of PAMI* **35** 1872–1886.

- [10] BRUNA, J., MALLAT, S., BACRY, E. and MUZY, J.-F. (2014). Supplement to “Intermittent process analysis with scattering moments.” DOI:[10.1214/14-AOS1276SUPP](https://doi.org/10.1214/14-AOS1276SUPP).
- [11] CASTAING, B. (2002). Lagrangian and Eulerian velocity intermittency. *Eur. Phys. J. B* **29** 357–358.
- [12] CHANAL, O., CHABAUD, B., CASTAING, B. and HEBRAL, B. (2000). Intermittency in a turbulent low temperature gaseous helium jet. *Eur. Phys. J. B* **17** 309–317.
- [13] CHUDACEK, V., ANDEN, J., MALLAT, S., ABRY, P. and DORET, M. (2014). Scattering transform for intrapartum fetal heart rate variability fractal analysis: A case-control study. *IEEE Trans. Biomed. Eng.* **61** 1100–1108.
- [14] DELOUR, J., MUZY, J. F. and ARNEODO, A. (2001). Intermittency of 1d velocity spatial profiles in turbulence: A magnitude cumulant analysis. *Eur. Phys. J. B* **23** 243.
- [15] FRISCH, U. (1995). *Turbulence: The Legacy of A. N. Kolmogorov*. Cambridge Univ. Press, Cambridge. [MR1428905](https://doi.org/10.1017/CBO9780511524757)
- [16] HANSEN, L. P. (1982). Large sample properties of generalized method of moments estimators. *Econometrica* **50** 1029–1054. [MR0666123](https://doi.org/10.2307/2331133)
- [17] JAFFARD, S. (1997). Multifractal formalism for functions part I: Results valid for all functions. *SIAM J. Math. Anal.* **28** 944–970.
- [18] JAFFARD, S. (1997). Multifractal formalism for functions part II: Self-similar functions. *SIAM J. Math. Anal.* **28** 971–998.
- [19] JAFFARD, S. (2001). Wavelet expansions, function spaces and multifractal analysis. In *Twentieth Century Harmonic Analysis—a Celebration (Il Ciocco, 2000)*. *NATO Sci. Ser. II Math. Phys. Chem.* **33** 127–144. Kluwer Academic, Dordrecht. [MR1858782](https://doi.org/10.1007/978-1-4020-0311-1_10)
- [20] JAFFARD, S., LASHERMES, B. and ABRY, P. (2007). Wavelet leaders in multifractal analysis. In *Wavelet Analysis and Applications* 201–246. Birkhäuser, Basel. [MR2297921](https://doi.org/10.1007/978-3-0301-4792-1_10)
- [21] JAFFARD, S. and MEYER, Y. (1996). Wavelet methods for pointwise regularity and local oscillations of functions. *Mem. Amer. Math. Soc.* **123** x+110. [MR1342019](https://doi.org/10.1090/S0025-5718-1996-0086113-0)
- [22] KAHANE, J. P. and PEYRIERE, J. (1975). Sur Certaines Martingales de B. Mandelbrot. Université Paris XI, Département de mathématique.
- [23] KYPRIANOU, A. E. (2006). *Introductory Lectures on Fluctuations of Lévy Processes with Applications*. Springer, Berlin.
- [24] LECUN, Y., KAVUKCUOGLU, K. and FARABET, C. (2010). Convolutional networks and applications in vision. In *Circuits and Systems (ISCAS), Proceedings of 2010 IEEE International Symposium on* 253–256. IEEE.
- [25] MALLAT, S. (2012). Group invariant scattering. *Comm. Pure Appl. Math.* **65** 1331–1398. [MR2957703](https://doi.org/10.1002/cpa.20858)
- [26] MANDELBROT, B. B. (1969). On intermittent free turbulence. In *Turbulence of Fluids and Plasmas*. Interscience, New York.
- [27] MANDELBROT, B. B. (1999). Intermittent turbulence in self-similar cascades: Divergence of high moments and dimension of the carrier. In *Multifractals and 1/f Noise* 317–357. Springer, New York.
- [28] MCFADDEN, D. (1989). A method of simulated moments for estimation of discrete response models without numerical integration. *Econometrica* **57** 995–1026. [MR1014539](https://doi.org/10.2307/2331133)
- [29] MUZY, J. F. and BACRY, E. (2002). Multifractal stationary random measures and multifractal random walks with log infinitely divisible scaling laws. *Phys. Rev. E* **66** 056121.

- [30] MUZY, J.-F., BACRY, E. and ARNEODO, A. (1993). Multifractal formalism for fractal signals: The structure-function approach versus the wavelet-transform modulus-maxima method. *Phys. Rev. E* **47** 875.
- [31] MUZY, J. F., DELOUR, J. and BACRY, E. (2000). Modeling fluctuations of financial time series: From cascade process to stochastic volatility model. *Eur. Phys. J. B* **17** 537–548.
- [32] OPPENHEIM, G., DOUKHAN, P. and TAQQU, M. S. (2003). *Theory and Applications of Long-Range Dependence*. Birkhäuser, Boston, MA. [MR1956041](#)
- [33] ROBERT, C. and ROSENBAUM, M. (2011). A new approach for the dynamics of ultra high frequency data: The model with uncertainty zones. *J. Financ. Econom.* **9** 344–366.
- [34] SELESNICK, I. W., BARANIUK, R. G. and KINGSBURY, N. C. (2005). The dual-tree complex wavelet transform. *IEEE Signal Process. Mag.* **22** 123–151.
- [35] SIFRE, L. and MALLAT, S. (2012). Combined scattering for rotation invariant texture analysis. In *European Symposium on Artificial Neural Networks*.
- [36] WENDT, H., ABRY, P. and JAFFARD, S. (2007). Bootstrap for empirical multifractal analysis. *IEEE Signal Process. Mag.* **24** 38–48.
- [37] WENDT, H., ROUX, S. G., ABRY, P. and JAFFARD, S. (2009). Wavelet leaders and bootstrap for multifractal analysis of images. *Signal Proces.* **89** 1100–1114.
- [38] YAGLOM, A. M. (1966). The influence of fluctuations in energy dissipation on the shape of turbulence characteristics in the inertial interval. *Soviet Physics Dokkl.* **11** 26.
- [39] YOSHIMATSU, K., SCHNEIDER, K., OKAMOTO, N., KAWAHARA, Y. and FARGE, M. (2011). Intermittency and geometrical statistics of three-dimensional homogeneous magnetohydrodynamic turbulence: A wavelet viewpoint. *Phys. Plasmas* **18** 092304.

J. BRUNA
 COURANT INSTITUTE OF MATHEMATICAL SCIENCES
 DEPARTMENT OF COMPUTER SCIENCE
 715 BROADWAY
 NEW YORK, NEW YORK 10012
 USA
 E-MAIL: bruna@cims.nyu.edu

S. MALLAT
 DEPARTEMENT D'INFORMATIQUE
 ÉCOLE NORMALE SUPÉRIEURE
 45 RUE D'ULM
 PARIS 75005
 FRANCE
 E-MAIL: mallat@cmap.polytechnique.fr

E. BACRY
 J.-F. MUZY
 CENTRE DES MATHÉMATIQUES APPLIQUÉES
 ÉCOLE POLYTECHNIQUE
 ROUTE DE SACLAY
 PALAISEAU 91128
 FRANCE
 E-MAIL: bacry@cmap.polytechnique.fr
muzy@univ-corse.fr